Eur. Phys. J. D **39**, 5–12 (2006)
DOI: 10.1140/epjd/e2006-00066-6

THE EUROPEAN PHYSICAL JOURNAL D

# M1-E2 interference in the Zeeman effect of the 461.5 nm line of Bi I

S. Werbowy, J. Kwela[a], R. Drozdowski, and J. Heldt

Institute of Experimental Physics, University of Gdansk, Wita Stwosza 57, 80-952 Gdańsk, Poland

Received 5 July 2005 / Received in final form 16 November 2005
Published online 28 March 2006 – 

**Abstract.** Studies of the interference effect in the mixed-type forbidden line 461.5 nm are reported. A special computer program considering the M1-E2 interference was designed to obtain the predicted contour of the Zeeman structure of the line. By variation of free parameters, describing the line shape and the electric-quadrupole admixture, the calculated profiles were fitted into the recorded spectra. The E2 admixture found is $(7.4 \pm 0.4)\%$. Our result is compared with recent theories and other experiments.

**PACS.** 32.10.Fn Fine and hyperfine structure – 32.60.+i Zeeman and Stark effects – 32.70.Fw Absolute and relative intensities – 31.15.Ct Semi-empirical and empirical calculations (differential overlap, Hückel, PPP methods, etc.)

## 1 Introduction

The $6s^2 6p^3$ ground configuration of bismuth gives rise to five levels $^4S_{3/2}$, $^2P_{3/2,1/2}$ and $^2D_{5/2,3/2}$. Since electric-dipole (E1) transitions between the states of the same parity are forbidden, all the levels of the $6s^2 6p^3$ configuration are metastable. Weak magnetic-dipole (M1) and electric-quadrupole (E2) transitions between these levels are permitted in the second-order radiation theory.

For strong transitions, the recently calculated theoretical decay rates are in reasonable agreement with experiment, but in the case of weak forbidden transitions the predictions often disagree with the experimental data. This results from the fact that weak transition rates are particularly sensitive to even small modifications to the wave functions, and a careful choice of the theoretical method is required.

For the Bi I spectrum, neither LS nor $jj$ coupling is adequate. The intermediate coupling in the fine structure of $6s^2 6p^3$ configuration in single configuration approximation has been studied by several authors [1–3]. A complete list of M1 and E2 transition probabilities in $6s^2 6p^3$ configuration of Bi I has been published in [3].

The most extensive multiconfiguration calculations of multipole transition rates for states within $6s^2 6p^3$ configuration of bismuth have been performed by Biémont and Quinet [4], by the use of the HFR method. The energies obtained in HFR calculations appear to be in very good agreement with the experiment, but the agreement with the experimental data concerning multipole transition rates is not that satisfactory. For instance, the experimental transition probability $A(^2D_{3/2} - ^4S_{3/2}) = 22.5 \pm 1.4\ s^{-1}$ [5] is almost 50% lower than the theoretical result. Furthermore, there is also a large discrepancy between the measured and calculated admixtures of E2 radiation in mixed transitions (see Tab. 1).

**Table 1.** Experimental and theoretical results for E2 admixture in mixed M1+E2 transitions in Bi I.

| Transition | $\lambda$(nm) | E2 admixture (%) | |
|---|---|---|---|
| | | Experiment | HFR theory[d] |
| $^2P_{3/2} \rightarrow {}^2D_{3/2}$ | 459.7 | $2.5 \pm 0.5$[a] | 3.3 |
| $^2P_{1/2} \rightarrow {}^4S_{3/2}$ | 461.5 | $6.5 \pm 0.5$[a] | 23 |
| $^2P_{3/2} \rightarrow {}^2D_{5/2}$ | 564.0 | $28 \pm 3$[b] | 34 |
| $^2D_{5/2} \rightarrow {}^4S_{3/2}$ | 647.6 | $16 \pm 1$[a] | 35 |
| | | $17 \pm 1$[c] | |
| $^2D_{3/2} \rightarrow {}^4S_{3/2}$ | 875.5 | $2.25 \pm 0.5$[b] | 1.3 |
| | | $1 \pm 1$[c] | |

[a] Reference [6], [b] reference [7], [c] reference [8], [d] reference [4].

In a theoretical study of forbidden lines Miliańczuk [9], Gerjuoy [10] and Shortley et al. [11] considered the transitions allowed for both magnetic-dipole and electric-quadrupole types of radiation. They pointed out that the intensity of Zeeman patterns of mixed multipole lines is not a simple sum of two contributions for M1 and E2 radiations taken in proportion to their transition probabilities, but should be modified by an interference term. This interference effect was for the first time ever observed experimentally by Jenkins and Mrozowski [12], for the line 733.2 nm of lead (lead in natural composition of isotopes was used). This line was reinvestigated using the even

[a] e-mail: fizjk@univ.gda.pl

isotope of lead [13]. The M1-E2 interference was also found for transitions with hyperfine structure i.e. for two lines 461.5 nm [14,15] and 647.6 nm [16] of bismuth. Similar observations have been made for the Te I line using Fourier transform spectroscopy [17]. The M1-E2 interference in Bi I lines has also been observed in absorption by means of the Faraday effect [8].

Dembinski et al. [15] derived detailed formulae for the radiation intensity of Zeeman components for mixed M1+E2 forbidden lines. It follows from these studies that the intensity of $\Delta M = \pm 1$ Zeeman components changes when observation is changed from transversal to longitudinal direction. This is due to the contribution from the interference between M1 and E2 radiations that are emitted with varying phases in different directions. A similar interference effect occurs between magnetic-quadrupole (M2) and electric-dipole (E1) radiations. Mixed forbidden transitions permitted simultaneously for both M2, and E1 enforced by the nuclear spin radiations, were theoretically predicted by Garstang [18] and Mizushima [19] for two-electron atoms with nuclear magnetic moment $I \neq 0$.

The M1-E2 interference effect in emission spectra produces the difference between the intensities of $\Delta M = \pm 1$ Zeeman patterns observed in longitudinal and transverse directions. This phenomenon was used in a series of experiments for precise determination of the electric-quadrupole admixture in forbidden lines. At the beginning of these studies, the intensities of certain groups of Zeeman patterns taken from the spectra obtained in longitudinal and transverse directions of observations (for $\sigma$ and $\pi$ polarizations), using photographic-photometry, were compared with calculations for varying E2 admixture. The magnetic field and Fabry-Perot spacers were selected in such a way that no overlap of different groups of Zeeman components was present [15,16,20]. Later, the time consuming photographic-photometry with all its uncertainties was replaced by a simple visual comparison, to find the best match between the experimental microphotometer trace and a series of calculated profiles for varying E2 admixture [6,7,21].

Currently, the development of the computer technique allows us to analyze fully the information contained in the recorded spectra. Since past attempts to estimate the E2 admixture in the 461.5 nm line gave results strongly different from the recent theory (see Tab. 1 and Refs. [6,14,15]), it seemed interesting to reexamine this line with the aid of our computer technique by using the previously obtained experimental data (photographic plates) [14].

## 2 Experiment

A standard experimental arrangement for observation of the Zeeman effect of forbidden lines described in detail in [14] was used. In brief, electrodeless discharge tube powered by an rf generator (100 MHz) was the source of forbidden lines. The high resolution spectral apparatus consisted of a silver-coated Fabry-Perot étalon (with 1.19 mm spacer) and a Hilger-Engris grating spectrograph. The light source was placed in the 20.4 cm gap of a Harvey-Wells magnet (30.5 cm diameter) producing a field up to 7 kG. The magnetic field was measured with an accuracy of 2% by the use of a gaussmeter. A Glan prism was used to separate the $\sigma$ and $\pi$ Zeeman components in the perpendicular view.

The spectra were recorded on Kodak 103a-O and 103a-F photographic plates. The exposure time was selected so as to keep the blackening of the photographic plates in a linear range. In addition, we analyzed all the available interferometric orders, to be sure that overexposure of films (in our case less prominent higher orders) does not play any role in the analysis of the spectra.

The spectra were converted into a digital form with a Carl Zeiss MD 100 microdensitometer. The plate with the recorded interferometric picture of the length of about 1 cm was shifted by a microdensitometer, step by step, with very small speed ($\sim$0.02 mm/s). The precision of each step could be adjusted within a range of 0.001 mm. All the time the plate was illuminated from the bottom by white light focused by an arrangement of lenses. The image was projected with severalfold enlargement on a screen and observed through a slit ($0.05 \times 5$ mm) by a photocell recording photocurrent proportional to the transmittance of the plate. The analog output of the microdensitometer was connected to the analog-to-digital converter card installed in the PC computer.

## 3 Theory

The general theory of the M1-E2 interference effect is scattered over various papers [9,10,15,22] and monographs (e.g. [23]).

Let $|a\rangle$ and $|b\rangle$ be two atomic states. The spontaneous transition probability $A_{ab}$ for a single photon emission with polarization $\overrightarrow{e}$ and momentum $\overrightarrow{k} = (\omega/c)\overrightarrow{n}$ ($\overrightarrow{n}$ is unit propagation vector) is given by [24]

$$A_{ab} = |\langle b|\widehat{U}(\overrightarrow{k}, \overrightarrow{e})|a\rangle|^2, \tag{1}$$

where an interaction energy operator $\widehat{U}(\overrightarrow{k}, \overrightarrow{e})$ expanded into multipole moments becomes

$$\widehat{U}(\overrightarrow{k}, \overrightarrow{e}) = \sum_{J,q} \left(\overrightarrow{e}^{*} \cdot \overrightarrow{Y}^{(0)}_{Jq}(\overrightarrow{n})\right) \widehat{u}^{(0)}_{Jq}(\overrightarrow{k}, \overrightarrow{e}) + \sum_{J,q} \left(\overrightarrow{e}^{*} \cdot \overrightarrow{Y}^{(1)}_{Jq}(\overrightarrow{n})\right) \widehat{u}^{(1)}_{Jq}(\overrightarrow{k}, \overrightarrow{e}). \tag{2}$$

The spherical vector $\overrightarrow{Y}^{(\lambda)}_{Jq}$ characterizes a photon with angular momentum $J$, its $\widehat{z}$ component $q$ and parity $P = (-1)^{J+\lambda+1}$, where $\lambda$ may assume values 1 or 0 for electric or magnetic multipoles respectively. In expression (2) the transversality condition $\overrightarrow{n} \cdot \overrightarrow{e} = 0$ was imposed.

In the non-relativistic limit, general forms of matrix elements of operators for electric and magnetic multipole

transitions, in Gauss gauge, are given by:

$$\langle b|\widehat{u}^{(1)}_{Jq}(\overrightarrow{k},\overrightarrow{e})|a\rangle = N(\omega,J)\langle b|\widehat{Q}^{(1)}_{Jq}|a\rangle \quad (3)$$

$$\widehat{Q}^{(1)}_{Jq} = ea_0^J C^{(J)}_q(\overrightarrow{n}) \quad (4)$$

and

$$\langle b|\widehat{u}^{(0)}_{Jq}(\overrightarrow{k},\overrightarrow{e})|a\rangle = iN(\omega,J)\langle b|\widehat{\mu}^{(0)}_{Jq}|a\rangle \quad (5)$$

$$\widehat{\mu}^{(0)}_{Jq} = \frac{2\mu_B}{J+1}\nabla(C^{(J)}_q(\overrightarrow{n}))(\overrightarrow{L}+(J+1)\overrightarrow{S}), \quad (6)$$

where $C^{(J)}_q(\overrightarrow{n}) = \sqrt{4\pi/(2J+1)}Y^*_{Jq}(\overrightarrow{n})$ are Racah tensors, $a_0$ is Bohr radius and $\mu_B$ is Bohr magneton. In equations (3) and (5), $N(\omega,J)$ denotes

$$N(\omega,J) = (-i)^J\sqrt{\frac{2}{\hbar}}\sqrt{\frac{J+1}{J}}\frac{\sqrt{2J+1}}{(2J+1)!!}\Big(\frac{\omega}{c}\Big)^{J+1/2}. \quad (7)$$

Let us limit our attention to the M1 and E2 contributions. Then substituting (2) into (1) yields

$$\begin{aligned} a^{Total}_{ab}(M\to M') = &\sum_{q=-1}^{1}|(\overrightarrow{e}^*\cdot\overrightarrow{Y}^{(0)}_{1q}(\overrightarrow{n}))|^2 a^{M1}_{ab}(q) \\ &+\sum_{q=-2}^{2}|(\overrightarrow{e}^*\cdot\overrightarrow{Y}^{(1)}_{2q}(\overrightarrow{n}))|^2 a^{E2}_{ab}(q) \\ &+2\mathrm{Re}\Bigg\{\sum_{q=-1}^{1}\Big((\overrightarrow{e}\cdot\overrightarrow{Y}^{*(0)}_{1q}(\overrightarrow{n}))(\overrightarrow{e}^*\cdot\overrightarrow{Y}^{(1)}_{2q}(\overrightarrow{n}))\Big) \\ &\times\langle b|\widehat{u}^{*(0)}_{1q}(\overrightarrow{k},\overrightarrow{e})|a\rangle\langle b|\widehat{u}^{(1)}_{2q}(\overrightarrow{k},\overrightarrow{e})|a\rangle\Bigg\}. \end{aligned} \quad (8)$$

Expression (8) shows that different magnetic and electric multipoles interfere. Therefore the transition probability for mixed transitions is not a simple sum of independent terms describing well-known pure multipole radiation of electric and magnetic type:

$$a^{M1}_{ab}(q) = |\langle b|\widehat{u}^{(0)}_{1q}(\overrightarrow{k},\overrightarrow{e})|a\rangle|^2 = \frac{4}{3\hbar}\Big(\frac{\omega}{c}\Big)^3\Big|\langle b|\widehat{\mu}^{(0)}_{1q}|a\rangle\Big|^2 \quad (9)$$

$$a^{E2}_{ab}(q) = |\langle b|\widehat{u}^{(1)}_{2q}(\overrightarrow{k},\overrightarrow{e})|a\rangle|^2 = \frac{1}{15\hbar}\Big(\frac{\omega}{c}\Big)^5\Big|\langle b|\widehat{Q}^{(1)}_{2q}|a\rangle\Big|^2. \quad (10)$$

However, the cross term vanishes after integration over photon polarizations and directions of observation. Then the interference can be observed only when various components of the atomic line (corresponding to different M', M) are separated with respect to wavelength by means of the magnetic field.

Let us calculate the scalar product $\overrightarrow{e}^*\cdot\overrightarrow{Y}^{(\lambda)}_{Jq}(\overrightarrow{n})$ connecting the states of polarization of the emitted radiation with the selection rules for $q$. Vectors $\overrightarrow{Y}^{(\lambda)}_{Jq}(\overrightarrow{n})$ are related to the vector spherical harmonics as follows

$$\overrightarrow{Y}^{(0)}_{Jq}(\overrightarrow{n}) = \overrightarrow{Y}_{JJq}(\overrightarrow{n}) \quad (11)$$

$$\overrightarrow{Y}^{(1)}_{Jq}(\overrightarrow{n}) = -i\overrightarrow{n}\times\overrightarrow{Y}^{(0)}_{Jq}(\overrightarrow{n}) \quad (12)$$

and by definition

$$\overrightarrow{Y}_{JlM}(\overrightarrow{n}) = \sum_{mq}Y_{lm}(\overrightarrow{n})\overrightarrow{e}_q(lm1q|l1JM). \quad (13)$$

In (13), $(lm1q|l1JM)$ are Clebsch-Gordan coefficients and $e_q$ denote the irreducible tensor components of the polarization vector [25].

The factors $\overrightarrow{e}^*\cdot\overrightarrow{Y}^{(\lambda)}_{Jq}(\overrightarrow{n})$ can then be written in terms of irreducible tensor components of $\overrightarrow{n}$, $\overrightarrow{e}$ and $\overrightarrow{n}\times\overrightarrow{e}$ vectors, to obtain

$$\begin{aligned} \Big(\overrightarrow{e}^*\cdot\overrightarrow{Y}^{(0)}_{10}(\overrightarrow{n})\Big) &= \frac{i}{4}\sqrt{\frac{6}{\pi}}(\overrightarrow{n}\times\overrightarrow{e})_0 \\ \Big(\overrightarrow{e}^*\cdot\overrightarrow{Y}^{(0)}_{1\pm1}(\overrightarrow{n})\Big) &= \frac{i}{4}\sqrt{\frac{6}{\pi}}(\overrightarrow{n}\times\overrightarrow{e})_{\pm1} \end{aligned} \quad (14)$$

for magnetic-dipole, and

$$\begin{aligned} \Big(\overrightarrow{e}^*\cdot\overrightarrow{Y}^{(1)}_{20}(\overrightarrow{n})\Big) &= \frac{1}{2}\sqrt{\frac{15}{2\pi}}n_0e_0 \\ \Big(\overrightarrow{e}^*\cdot\overrightarrow{Y}^{(1)}_{2\pm1}(\overrightarrow{n})\Big) &= \frac{1}{2}\sqrt{\frac{5}{2\pi}}(n_0e_{\pm1}+n_{\pm1}e_0) \\ \Big(\overrightarrow{e}^*\cdot\overrightarrow{Y}^{(1)}_{2\pm2}(\overrightarrow{n})\Big) &= \frac{1}{2}\sqrt{\frac{5}{\pi}}n_{\pm1}e_{\pm1} \end{aligned} \quad (15)$$

for electric-quadrupole contributions, respectively. Equations (14) and (15) express the angular distribution of multipole radiation in any direction holding the relation between directions of polarization and propagation of the photon.

Let us assume that $|a\rangle$ and $|b\rangle$ are eigenstates of the $\widehat{z}$ components of the angular momentum and are labelled by the set of quantum numbers $(\gamma JIFM_F)$. The magnetic field is directed along the $\widehat{z}$ axis and the unit vectors $\overrightarrow{e}$ and $\overrightarrow{n}$ are determined by:

$$\overrightarrow{n} = \widehat{y}\sin\theta+\widehat{z}\cos\theta \quad (16)$$

$$\overrightarrow{e} = \varepsilon_2\widehat{x}+\varepsilon_1(\widehat{z}\sin\theta-\widehat{y}\cos\theta), \quad (17)$$

where $\theta$ is the angle between the direction of the magnetic field and the direction of observation, and parameters $\varepsilon_1$, $\varepsilon_2$ are introduced in order to distinguish the contributions due to the two mutually orthogonal directions of polarization.

Let us assume that $\varepsilon_1 = \cos\alpha$ and $\varepsilon_2 = \exp(i\beta)\sin\alpha$. Then, the set ($\alpha = \pi/4$, $\beta = \pm\pi/2$) corresponds to the observation of circular polarized radiation, arbitrary $\alpha$ and $\beta$ are adequate to the elliptically polarized light, whereas $\beta = 0$ corresponds to the radiation polarized linearly at the angle $\alpha$ to the $zy$-plane (see Fig. 1).

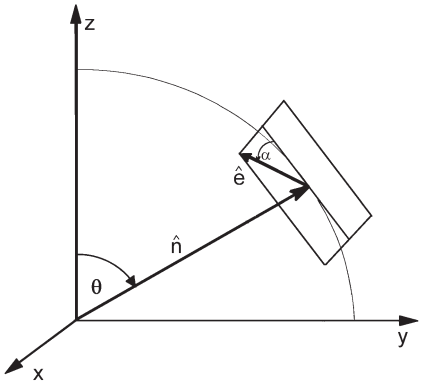


**Fig. 1.** The system of two mutually orthogonal unit vectors $\hat{\mathbf{n}}$ and $\hat{\mathbf{e}}$ determining the direction of propagation and polarization of the emitted photon respectively.

With this convention, the coefficients $b_{Jq}^{(\lambda)} = \sqrt{16\pi}(\overrightarrow{e}^{*} \cdot \overrightarrow{Y}_{Jq}^{(\lambda)}(\overrightarrow{n}))$ become

$$\begin{aligned}
b_{10}^{(0)} &= -i\sqrt{6}\Big[\varepsilon_2\Big]\sqrt{1-x^2} \\
b_{1\pm1}^{(0)} &= \mp i\sqrt{3}\Big[\varepsilon_1 \pm i\varepsilon_2 x\Big] \\
b_{20}^{(1)} &= \sqrt{30}\Big[\varepsilon_1\Big]x\sqrt{1-x^2} \\
b_{2\pm1}^{(1)} &= i\sqrt{5}\Big[\varepsilon_1(2x^2-1) \pm i\varepsilon_2 x\Big] \\
b_{2\pm2}^{(1)} &= \sqrt{5}\Big[\varepsilon_1 x + i\varepsilon_2\Big]\sqrt{1-x^2}.
\end{aligned} \tag{18}$$

Similarly, the products $b_{Jq}^{*(\lambda)} b_{J'q}^{(\lambda')}$ can be written as

$$\begin{aligned}
|b_{10}^{(0)}|^2 &= 6\Big[|\varepsilon_2|^2\Big](1-x^2) \\
|b_{1\pm1}^{(0)}|^2 &= 3\Big[|\varepsilon_1|^2 + |\varepsilon_2|^2 x^2 \pm i(\varepsilon_1^*\varepsilon_2 - \varepsilon_2^*\varepsilon_1)x\Big] \\
|b_{20}^{(1)}|^2 &= 30\Big[|\varepsilon_1|^2\Big](1-x^2)x^2 \\
|b_{2\pm1}^{(1)}|^2 &= 5\Big[|\varepsilon_1|^2(2x^2-1)^2 + |\varepsilon_2|^2 x^2 \\
&\qquad \pm i(\varepsilon_1^*\varepsilon_2 - \varepsilon_2^*\varepsilon_1)(2x^2-1)x\Big] \\
|b_{2\pm2}^{(1)}|^2 &= 5(1-x^2)\Big[|\varepsilon_1|^2 x^2 + |\varepsilon_2|^2 \\
&\qquad \pm i(\varepsilon_1^*\varepsilon_2 - \varepsilon_2^*\varepsilon_1)x\Big] \\
b_{1\pm1}^{*(0)} b_{2\pm1}^{(1)} &= \mp\sqrt{15}\Big[|\varepsilon_1|^2(2x^2-1) + |\varepsilon_2|^2 x^2 \\
&\qquad \pm ix(\varepsilon_1^*\varepsilon_2 - \varepsilon_2^*\varepsilon_1(2x^2-1))\Big],
\end{aligned} \tag{19}$$

where $x = \cos\theta$ ($x = 0$ for transverse and $x = 1$ for longitudinal directions of observation, respectively).

For all the contributions to the total transition probability, expressions (19) connect the states of polarization of the emitted light with the selection rules for $\Delta M$ as shown in Table 2. The states of polarization presented in the table correspond to the maxima of the absolute values of $b_{Jq}^{*(\lambda)} b_{J'q}^{(\lambda')}$. Numerical values of products $b_{Jq}^{*(\lambda)} b_{J'q}^{(\lambda')}$ are summarized in Table 3.

In the absence of the magnetic field the atomic states are obtained by diagonalization of the hyperfine structure

**Table 2.** Polarization rules for Zeeman components.

| | Longitudinal observation | | | Transverse observation | | |
|---|---|---|---|---|---|---|
| $\Delta M$ | M1 | E2 | M1-E2 | M1 | E2 | M1-E2 |
| 2 | – | – | – | – | $\sigma$ | – |
| 1 | right circular | right circular | right circular | $\pi$ | $\pi$ | $\pi$ |
| 0 | – | – | – | $\sigma$ | – | – |
| –1 | left circular | left circular | left circular | $\pi$ | $\pi$ | $\pi$ |
| –2 | – | – | – | – | $\sigma$ | – |

**Table 3.** Numerical values of products $b_{Jq}^{*(\lambda)}(\theta) b_{J'q}^{(\lambda')}(\theta)$.

| | Longitudinal observation | | | Transverse observation | | |
|---|---|---|---|---|---|---|
| $q$ | $\lvert b_{1q}^{(0)}\rvert^2$ | $\lvert b_{2q}^{(1)}\rvert^2$ | $(b_{1q}^{*(0)} b_{2q}^{(1)})$ | $\lvert b_{1q}^{(0)}\rvert^2$ | $\lvert b_{2q}^{(1)}\rvert^2$ | $(b_{1q}^{*(0)} b_{2q}^{(1)})$ |
| 2 | – | – | – | – | 5 | – |
| 1 | 3 | 5 | $-\sqrt{15}$ | 3 | 5 | $+\sqrt{15}$ |
| 0 | – | – | – | 6 | – | – |
| $-1$ | 3 | 5 | $+\sqrt{15}$ | 3 | 5 | $-\sqrt{15}$ |
| $-2$ | – | – | – | – | 5 | – |

Hamiltonian and are labelled by the set of quantum numbers $(\gamma, J, I, F)$. In the presence of the field, the atomic eigenstates can be expressed as linear combinations of the form:

$$|\psi_{M_F}\rangle = \sum_F C_{M_F F}^{\gamma} |\gamma, J, I, F, M_F\rangle. \tag{20}$$

The $C_{M_F F}^{\gamma}$ coefficients can be obtained by diagonalization of the Hamiltonian matrix with matrix elements given by

$$\begin{aligned}
\mathcal{H}_{F'M,FM} = \\
\delta_{F'F}\left(A\frac{C}{2} + \frac{B}{8}\frac{\frac{3}{4}C(C+1) - I(I+1)J(J+1)}{I\left(I-\frac{1}{2}\right)J\left(J-\frac{1}{2}\right)}\right) \\
+ \mu_B g_J H_{mag}\langle\gamma JIF'M|J_z^{(1)}|\gamma JIFM\rangle,
\end{aligned} \tag{21}$$

where the matrix element of $J_z^{(1)}$ can be calculated as

$$\begin{aligned}
\langle\gamma JIF'M_F|J_z^{(1)}|\gamma JIFM_F\rangle = (-1)^{F'-M_F+J+I+F+1} \\
\times\sqrt{(2F'+1)(2F+1)J(J+1)(2J+1)} \\
\times\begin{pmatrix} F' & 1 & F \\ -M_F & 0 & M_F \end{pmatrix}\begin{Bmatrix} F' & 1 & F \\ J & I & J \end{Bmatrix}.
\end{aligned} \tag{22}$$

In (21) $C = F(F+1) - I(I+1) - J(J+1)$, $A$ and $B$ are hyperfine structure constants and $g_J$ is the Landé factor.

Using the standard vector coupling technique [25], the matrix elements of $\widehat{u}_{kq}^{(\lambda)}$ operators for electric and magnetic multipole transitions can be written in terms of 3-$j$ and 6-$j$ symbols as

$$\langle\gamma' J' IF' M_F'|\widehat{u}_{kq}^{(\lambda)}|\gamma JIFM_F\rangle = \mathcal{S}_{qF'F}^{(k)}\langle\gamma' J'||\widehat{u}_k^{(\lambda)}||\gamma J\rangle, \tag{23}$$

where

$$\mathcal{S}^{(k)}_{qF'F} = (-1)^{F'-M'_F+J'+I+F+k}\sqrt{(2F'+1)(2F+1)} \times \begin{pmatrix} F' & k & F \\ -M'_F & q & M_F \end{pmatrix} \begin{Bmatrix} J' & F' & I \\ F & J & k \end{Bmatrix}. \quad (24)$$

Then, the transition probability can be expressed as

$$a^{Total}_{M'_F,M_F} = \frac{1}{16\pi}\Bigg[ \sum_{q=-1}^{1} |b^{(0)}_{1q}|^2 \Big|\langle\gamma' J'||\widehat{u}^{(0)}_1||\gamma J\rangle\Big|^2 |\mathcal{S}^{(1)}_{qM'_F M_F}|^2 + \sum_{q=-2}^{2} |b^{(1)}_{2q}|^2 \Big|\langle\gamma' J'||\widehat{u}^{(1)}_2||\gamma J\rangle\Big|^2 |\mathcal{S}^{(2)}_{qM'_F M_F}|^2 + 2\mathrm{Re}\Bigg\{ \sum_{q=-1}^{1} (b^{*(0)}_{1q} b^{(1)}_{2q}) \langle\gamma' J'||\widehat{u}^{(0)}_1||\gamma J\rangle \langle\gamma' J'||\widehat{u}^{(1)}_2||\gamma J\rangle \times \mathcal{S}^{(1)}_{qM'_F M_F} \mathcal{S}^{(2)}_{qM'_F M_F} \Bigg\}\Bigg], \quad (25)$$

where $\mathcal{S}^{(k)}_{qM'_F M_F}$ denotes

$$\mathcal{S}^{(k)}_{qM'_F M_F} = \sum_{F',F} C^{*\gamma'}_{M'_F F'} \mathcal{S}^{(k)}_{qF'F} C^{\gamma}_{M_F F}. \quad (26)$$

The electric-quadrupole admixture in mixed transition is defined by

$$D = \frac{A^{E2}_{ab}}{A^{M1}_{ab} + A^{E2}_{ab}}, \quad (27)$$

where

$$A_{ab} = \sum_{M'_F,M_F} a_{ab}(M'_F \to M_F). \quad (28)$$

It is easy to show that definition (27) is equivalent to

$$D = \frac{|\langle\gamma' J'||\widehat{u}^{(1)}_2||\gamma J\rangle|^2}{|\langle\gamma' J'||\widehat{u}^{(0)}_1||\gamma J\rangle|^2 + |\langle\gamma' J'||\widehat{u}^{(1)}_2||\gamma J\rangle|^2}, \quad (29)$$

As a final step one may express the relative transition probability $\widetilde{a}^{Total}_{M'_F,M_F}$, defined as $\widetilde{a}^{Total}_{M'_F,M_F} = a^{Total}_{M'_F,M_F}/(A^{M1}_{ab} + A^{E2}_{ab})$ according to

$$\widetilde{a}^{Total}_{M'_F,M_F} = \frac{1}{16\pi}\Big[(1-D)|b^{(0)}_{1q}|^2 |\mathcal{S}^{(1)}_{M'_F M_F}|^2 + D|b^{(1)}_{2q}|^2 |\mathcal{S}^{(2)}_{M'_F M_F}|^2 + 2\sqrt{D(1-D)}(b^{*(0)}_{1q} b^{(1)}_{2q}) \mathcal{S}^{(1)}_{M'_F M_F} \mathcal{S}^{(2)}_{M'_F M_F}\Big]. \quad (30)$$

The relative intensities of Zeeman patterns observed in experiment are directly proportional to the relative transition probabilities $\widetilde{a}^{Total}_{M'_F,M_F}$.

| | $^2\mathrm{P}^0_{1/2}$ | $^4\mathrm{S}^0_{3/2}$ |
|---|---|---|
| $A$ | 376 | –14.9 |
| $B$ | 0 | –10.1 |
| $g_J$ | 0.667 | 1.650 |

**Table 4.** Values of the hyperfine structure constants $A$ and $B$ (in mK) and Landé $g_J$ factors used in our computations (see Refs. [26,27]).

Analysis of equations (25) and (19) makes it possible to determine the general features of the M1-E2 interference effect.

- The interference can be observed only when various components of the atomic line are separated as to wavelength. This is a consequence of the following orthogonality property for the 3-$j$ symbols

$$\sum_{M'_F,M_F} \begin{pmatrix} F' & 1 & F \\ -M'_F & q & M_F \end{pmatrix} \begin{pmatrix} F' & 2 & F \\ -M'_F & q & M_F \end{pmatrix} = 0. \quad (31)$$

- The interference does not change the state of polarization of the emitted radiation for all the directions of observation (see Tab. 2).
- The interference term, modifying the intensities of Zeeman components, can be positive or negative. It has different values for different components and changes with the direction of observation. The interference term changes its sign when observation is changed from transverse to longitudinal, but its absolute value remains the same (see Tab. 3).

## 4 The computer program

A direct observation of separate hfs Zeeman components is practically unachievable for conditions under which the hfs is barely resolved. What can be observed is an envelope of partially overlapping lines. We assumed that the observed contour is described by the following intensity distribution function:

$$I(\nu) = I_0(\nu) + \sum_i \frac{I_i}{1 + \alpha_1^2(\nu - \widetilde{\nu}_i)^2 + \alpha_2^4(\nu - \widetilde{\nu}_i)^4}, \quad (32)$$

where $I_0(\nu)$ describes the background noise, $I_i$ is the intensity of the $i$th Zeeman component directly proportional to the transition probability (30), $\widetilde{\nu}_i = \nu_i + \nu_0$ is the position of the component on the frequency axis ($\nu_0$ shifts the whole contour either left or right), and parameters $\alpha_1$, $\alpha_2$ describe the shape of the line. The function (32) is a convolution of Cauchy, Gauss and approximate Airy functions [28,29]. The Cauchy and Gauss functions describe the radiative and Doppler broadenings of the atomic line whereas the Airy profile is connected with instrumental broadening.

The first step in the computer analysis involves finding the position and the relative intensities of all the individual components. This procedure accepts the required atomic data of the investigated line: the magnitude of the external magnetic field $H_{mag}$, hyperfine structure constants A and B, Landé $g_J$ factors (see Tab. 4), and quantum numbers $I$ and $J$ for the two energy levels involved.

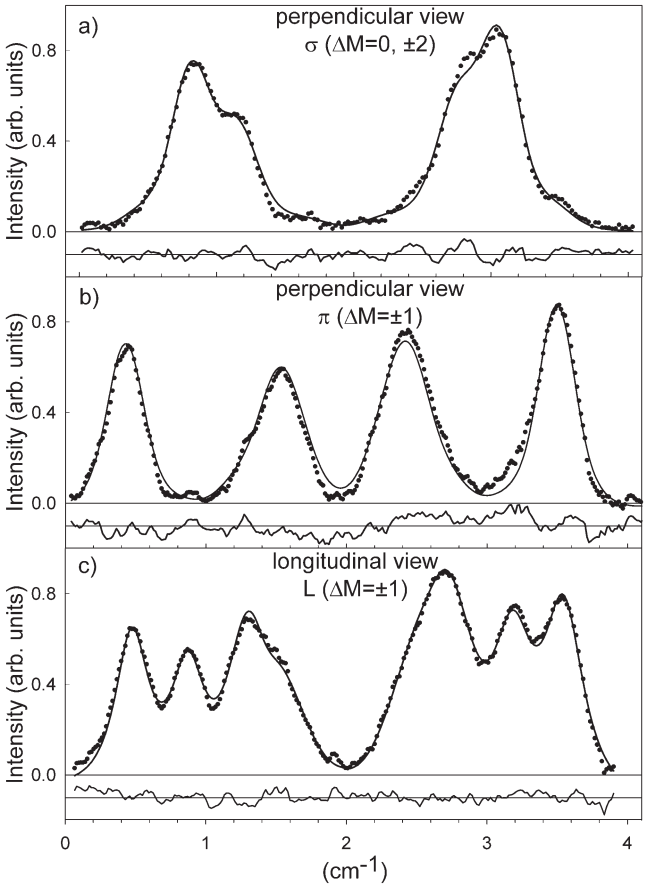


**Fig. 2.** Zeeman patterns of the 461.5 nm line at 5.0 kG for $\sigma$, $\pi$ and L-views. Black dots present microdensitometer traces. Solid lines are the computer-generated best fits obtained for $D = 7.7\%$. At the bottom of each picture the "error" curves present deviations between calculated and experimental profiles.

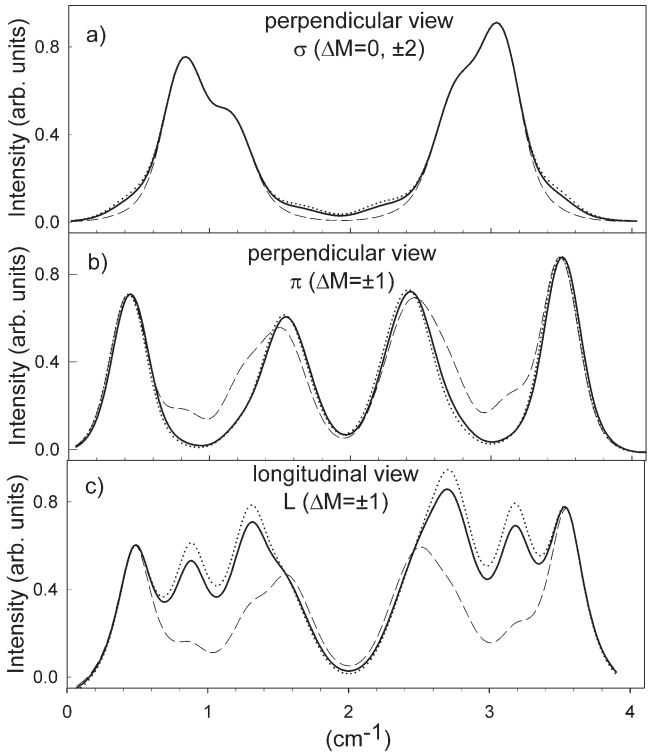


**Fig. 3.** Computer-generated contours for different values of the electric-quadrupole admixture $D$. Solid lines are the curves of the best fit obtained for $D = 7.7\%$. The dotted and dashed lines are calculated profiles for $D = 10\%$ and $D = 0\%$, respectively. Zeeman patterns were obtained for 5.0 kG magnetic field. All contours were normalized to the intensity of the first peaks maxima.

The next procedure sorts all the components according to the wave numbers and separates them into groups corresponding to $\pi$, $\sigma$ and L views. Then the intensity distribution function (32) is employed to calculate the sum of intensities at each point of the final pattern using estimated values for the electric-quadrupole admixture $D$ and line profile coefficients $\alpha_1$, $\alpha_2$.

In the next step, the least-square-fitting procedure is used. The simulated structure is fitted to the experimental curve recorded in digital form. The actual Fabry-Perot pattern has a variable dispersion, especially near the center of the fringe system, but the simulated structure is calculated with a linear dispersion. In order to avoid difficulty the experimental profile is linearized. Care is taken to keep the area under the interferometric curve constant in this procedure. After linearization the profile is normalized. Then, by variation of $D$ values and line shape parameters, the simulated contour is fitted to the experimental data. We used Marquardt's algorithm [30] in this procedure.

## 5 Results

The observations of the Zeeman effect were performed for four field values: 2.7, 3.8, 5.0 and 6.2 kG and for longitudinal and transverse directions of observation. As examples, Figures 2 and 4 show the recorded Zeeman structures of the line for two field values 5.0 and 6.2 kG. The observed line contours were analyzed using the least-square-fitting procedure described in Section 4. Black dots represent the experimental results and the solid lines are the computer best fits described by formula (32). The "error" curves at the bottom of each picture present the differences between the calculated and experimental contours.

We analyzed four or five interferometric orders for each value of the magnetic field. Our studies show that more precise results have been obtained for higher field values — it is caused by richer structures of the spectra. Moreover, more reliable results have been obtained from the analysis of the spectra for the longitudinal direction of observation (L-views). The reason for that can be explained by Figures 3 and 5. These figures present the computer simulations of the Zeeman patterns for varying values of the electric-quadrupole admixture $D$ (simulated shapes were normalized to the first peaks maxima). The presented figures show the sensitivity of the shape of the generated

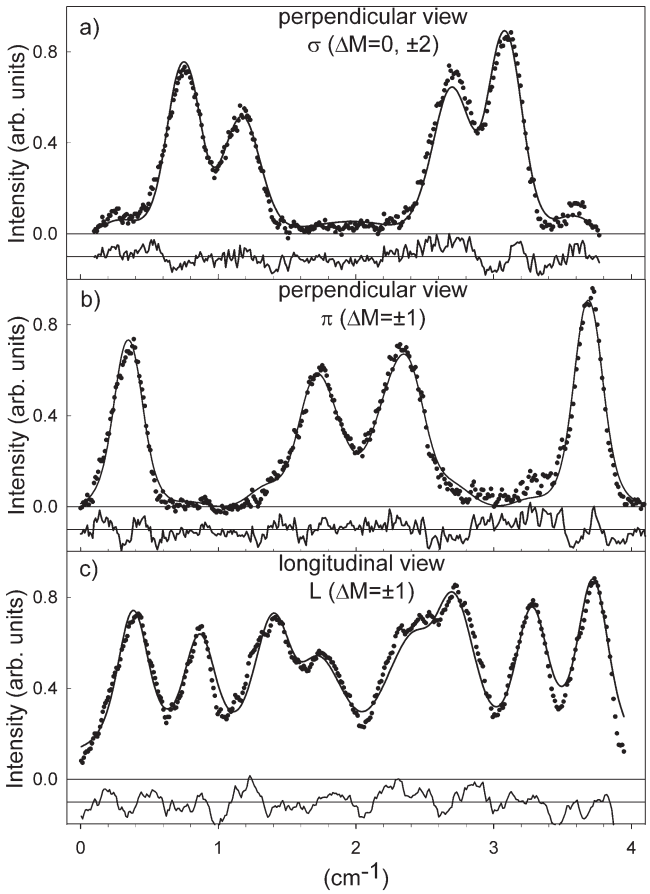


**Fig. 4.** Zeeman patterns of the 461.5 nm line at 6.2 kG for $\sigma$, $\pi$ and L-views. Black dots present microdensitometer traces. Solid lines are the computer-generated best fits obtained for $D = 7.3\%$. At the bottom of each picture the "error" curves present deviations between calculated and experimental profiles.

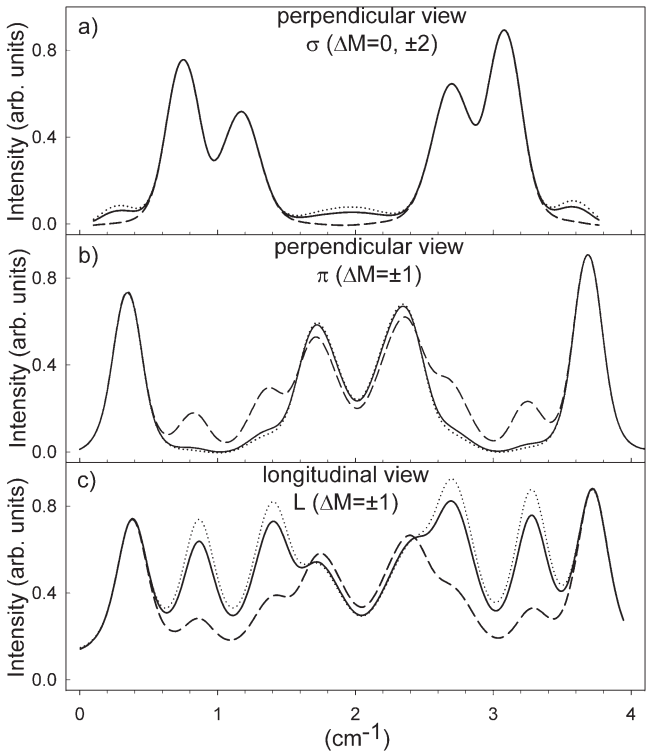


**Fig. 5.** Computer-generated contours for different values of the electric-quadrupole admixture $D$. Solid lines are the curves of the best fit obtained for $D = 7.3\%$. The dotted and dashed lines are calculated profiles for $D = 10\%$ and $D = 0\%$, respectively. Zeeman patterns were obtained for 6.2 kG magnetic field. All contours were normalized to the intensity of the first peaks maxima.

structure to the $D$ parameter changes; it is apparent that L-view is the most sensitive one.

The computer simulation yields $D = 7.7\%$ for the results presented in Figure 2 for 5.0 kG magnetic field and $D = 7.3\%$ for the results presented in Figure 4 obtained for 6.2 kG. All the obtained results for $D$ varied in the range of 6.4−8.4. The $\alpha_1$ parameter values obtained from the fitting procedure varied from 0.30 $\mathrm{cm}^{-1}$ to 0.41 $\mathrm{cm}^{-1}$, and the values of $\alpha_2$ varied in the range of 0.32−0.70 $\mathrm{cm}^{-1}$.

The weighted mean value from all our experimental results for different magnetic fields and studied interferometric orders was determined to be $D = (7.4 \pm 0.4)\%$. The error bar represents the standard deviation.

In Table 5 our result was compared with the experimental results of other authors and with theoretical predictions. Our value for $D$ is higher than the experimental result $D = (6.5 \pm 0.5)\%$ from [6], but not in disagreement. Other experimental results obtained earlier are significantly higher. There is also a large discrepancy between the value obtained by us and HFR predictions. As follows from Table 5, a very good agreement was achieved in semiempirical single-configuration calculations [32], where

**Table 5.** Experimental and theoretical results for percentage admixture of E2 radiation in mixed 461.5 nm line of Bi I.

| Experiment | Theory | Method of calculations |
|---|---|---|
| 20[a] | 10.1[e] | Single configuration approximation |
| $8 \div 9$[b] | 23[f] | Multi-configurational HFR |
| $10 \pm 0.8$[c] | 7.3[g] | Semiempirical |
| $6.5 \pm 0.5$[d] | | |
| $7.4 \pm 0.4$* | | |

[a] Reference [31]; [b] reference [14]; [c] reference [15]; [d] reference [6]; [e] reference [3]; [f] reference [4]; [g] reference [32]; * present work.

the Landman and Lurio intermediate-coupling wave functions [2] and experimental value for the radial integral $s_q$ of $r^2$ between single-electron states $s_q = 8.7ea_0^2$ from [8] were used.

## 6 Conclusion

We reexamined the E2 admixture measurement for the 461.5 nm line of Bi I. We found a large discrepancy between our value and the result predicted by multi-configurational HFR theory. On the other hand, our experimental value is in very good agreement with the result

of semiempirical calculations in the single-configuration approximation. It shows that the situation in calculations of transition probabilities is very complex. In the case of ground configuration of Bi I, the effect of configuration mixing is very weak, and limited inclusion into calculations admixtures of several selected configurations does not necessarily improve the agreement with experiment, even if the calculated energy levels agree better with observation.

This work was supported by the KBN Committee (Grant 127/E-335/S/2004).

## References

1. E.U. Condon, G.H. Shortley, *The theory of atomic spectra* (Cambridge University Press, Cambridge, 1963)
2. D.A. Landman, A. Lurio, Phys. Rev. A **1**, 1330 (1970)
3. R.H. Garstang, J. Res. Natl. Bur. Stand. A **68**, 61 (1964)
4. E. Biémont, P. Quinet, Phys. Scripta **54**, 36 (1996)
5. D. Patel, A.T. Pritt Jr, R.D. Coombe, J. Chem. Phys. **76**, 6449 (1982)
6. J. Czerwińska, J. Opt. Soc. Am. B **4**, 1349 (1987)
7. J. Czerwińska, S. Mrozowski, J. Opt. Soc. Am. B **8**, 940 (1990)
8. G.J. Roberts, P.E.G. Baird, M.W.S.M. Brimicombe, P.G.H. Sanders, D.R. Selby, D.N. Stacey, J. Phys. B **13**, 1389 (1980)
9. B. Miliańczuk, Bull. Acad. Pol. Sci. 430 (1935)
10. E. Gerjuoy, Phys. Rev. **60**, 233 (1941)
11. G.H. Shortley, L.H. Aller, J.G. Baker, D.H. Menzel, Astrophys. J. **93**, 178 (1941)
12. F.A. Jenkins, S. Mrozowski, Phys. Rev. **60**, 225 (1941)
13. M.E. Hults, J. Opt. Soc. Am. **56**, 1298 (1966)
14. J. Heldt, S. Mrozowski, J. Opt. Soc. Am. **60**, 467 (1970)
15. S.T. Dembiński, J. Heldt, L. Wolniewicz, J. Opt. Soc. Am. **62**, 555 (1972)
16. L. Augustyniak, J. Heldt, J. Bronowski, Phys. Scripta **12**, 157 (1975)
17. C. Morillon, J. Verges, Phys. Scripta **12**, 145 (1975)
18. R.H. Garstang, Astrophys. J. **148**, 579 (1967)
19. M. Mizushima, Phys. Rev. A **134**, 883 (1964)
20. J. Czub, J. Heldt, A. Kowalczyk, Acta Phys. Pol. A **44**, 609 (1973)
21. S. Mrozowski, J. Czerwińska, R. Drozdowski, J. Opt. Soc. Am. **10**, 607 (1993)
22. J. Heldt, J. Kwela, Act. Phys. Pol. A **66**, 63 (1984)
23. R.D. Cowen, *The theory of atomic structure and spectra*, (University of California Press, 1981)
24. A.I. Akhiezer, V.B. Berestetskii, *Quantum Electrodynamics* (Wiley, New York, 1965)
25. A.R. Edmonds, *Angular Momentum in Quantum mechanics* (Princeton, New Jersey, 1957)
26. L.O. Dickie, F.M. Kelly, Can. J. Phys. **45**, 2249 (1967)
27. R.S. Title, K.F. Smith, Phil. Mag. **5**, 1281 (1960)
28. H. Hühnermann, Dissertation, Philips-Universitat Marburg/Lahn, 1967
29. G. Müller, Dissertation, Technische Universität Berlin, 1974
30. D.W. Marquardt, J. Soc. Indust. Appl. Math. **11**, 431 (1963)
31. J. Heldt, J. Opt. Soc. Am. **58**, 1516 (1968)
32. P. Horodecki, J. Kwela, J.E. Sienkiewicz, Eur. Phys. J. D **6**, 435 (1999)